

ISSN 2072-5981
doi: 10.26907/mrsej



***magnetic
Resonance
in Solids***

Electronic Journal

Volume 26

Issue 2

Article No 24211

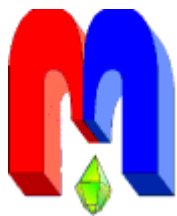
1-9 pages

June, 6

2024

doi: [10.26907/mrsej-24211](https://doi.org/10.26907/mrsej-24211)

<http://mrsej.kpfu.ru>
<https://mrsej.elpub.ru>



Established and published by Kazan University*
Endorsed by International Society of Magnetic Resonance (ISMAR)
Registered by Russian Federation Committee on Press (#015140),
August 2, 1996
First Issue appeared on July 25, 1997

© Kazan Federal University (KFU)†

"Magnetic Resonance in Solids. Electronic Journal" (MRSej) is a peer-reviewed, all electronic journal, publishing articles which meet the highest standards of scientific quality in the field of basic research of a magnetic resonance in solids and related phenomena.

Indexed and abstracted by
Web of Science (ESCI, Clarivate Analytics, from 2015), Scopus (Elsevier, from 2012), RusIndexSC (eLibrary, from 2006), Google Scholar, DOAJ, ROAD, CyberLeninka (from 2006), SCImago Journal & Country Rank, etc.

Editor-in-Chief

Boris **Kochelaev** (KFU, Kazan)

Honorary Editors

Jean **Jeener** (Universite Libre de Bruxelles, Brussels)

Raymond **Orbach** (University of California, Riverside)


Executive Editor

Yurii **Proshin** (KFU, Kazan)

mrsej@kpfu.ru



This work is licensed under a [Creative Commons Attribution-ShareAlike 4.0 International License](https://creativecommons.org/licenses/by-sa/4.0/).

 This is an open access journal which means that all content is freely available without charge to the user or his/her institution. This is in accordance with the [BOAI definition of open access](https://www.boai.ru/).

Technical Editors

Maxim **Avdeev** (KFU, Kazan)

Vadim **Tumanov** (KFU, Kazan)

Fail **Siraeu** (KFU, Kazan)

Editors

Vadim **Atsarkin** (Institute of Radio Engineering and Electronics, Moscow)

Yurij **Bunkov** (CNRS, Grenoble)

Mikhail **Eremin** (KFU, Kazan)

David **Fushman** (University of Maryland, College Park)

Hugo **Keller** (University of Zürich, Zürich)

Yoshio **Kitaoka** (Osaka University, Osaka)

Boris **Malkin** (KFU, Kazan)

Alexander **Shengelaya** (Tbilisi State University, Tbilisi)

Jörg **Sichelschmidt** (Max Planck Institute for Chemical Physics of Solids, Dresden)

Haruhiko **Suzuki** (Kanazawa University, Kanazawa)

Murat **Tagirov** (KFU, Kazan)

Dmitrii **Tayurskii** (KFU, Kazan)

Valentine **Zhikharev** (KNRTU, Kazan)

Invited Editor of Special Issue[‡]: Eduard Baibekov (KFU, Kazan)

* Address: "Magnetic Resonance in Solids. Electronic Journal", Kazan Federal University; Kremlevskaya str., 18; Kazan 420008, Russia

† In Kazan University the Electron Paramagnetic Resonance (EPR) was discovered by Zavoisky E.K. in 1944.

‡ Dedicated to Professor Boris Z. Malkin on the occasion of his 85th birthday

The optical and magnetic properties of CeO₂ nanoparticles doped with Er³⁺ ions[†]

M.S. Pudovkin¹, O.A. Morozov^{1,2}, S.L. Korableva¹, R.M. Rakhmatullin^{1,*}, V.V. Semashko^{1,2},
A.K. Ginkel¹, A.A. Rodionov¹, A.G. Kiiamov^{1,2}

¹Kazan State University, Kazan 420008, Russia

²Zavoisky Physical-Technical Institute, FRC Kazan Scientific Center of RAS, Kazan 420029,
Russia

*E-mail: rafail.rakhmatullin@kpfu.ru

(Received March 26, 2024; accepted May 30, 2024; published June 6, 2024)

The EPR spectroscopy and magnetization measurements were used to study the effect of annealing conditions on the local structure of Er³⁺ ions in CeO₂ : 1% Er³⁺ nanoparticles. The nanoparticles were synthesized using the coprecipitation technique from an aqueous solution of cerium nitrate and hexamethylenetetramine.

A correlation was found between the EPR spectra of the Er³⁺ ions, magnetization and luminescence, depending on the annealing atmosphere, which proved the crucial role of oxygen vacancies in the origin of magnetism in CeO₂ nanoparticles.

EPR lines due to trigonal centers were clearly detected in CeO₂ : 1% Er³⁺ nanoparticles annealed in a vacuum, while no such lines were found for similar nanoparticles annealed under argon or air atmospheres.

PACS: 75.75.-c, 76.30.Kg, 78.67.-n.

Keywords: CeO₂, nanoparticles, vacancies, EPR, trigonal centers.

1. Introduction

Cerium dioxide (CeO₂) nanoparticles (NPs) are promising materials for applications in various fields, including energy, catalysis, medicine, bio-imaging, and electronics [1–8]. The key feature of CeO₂ NPs is the ability to keep its fluorite-type structure at high concentrations of oxygen vacancies which defines the main applications of this material [9]. This property is related to the easy transition between the Ce⁴⁺ and Ce³⁺ oxidation states of cerium in CeO₂, which are accompanied by the formation of oxygen vacancies in the structure [10]. According to the publications from various research groups [11–15], doping CeO₂ NPs with rare earth ions increases the concentration of the oxygen vacancies. Indeed, the rare earth ions typically have an oxidation state of 3+, and they substitute for cerium ions in the 4+ oxidation state. To maintain charge balance, the vacancies can be formed, similar to those in the undoped CeO₂ NPs. The knowledge of the concentration and distribution of vacancies is essential for the efficient use of rare earth doped CeO₂ NPs. It has been found that the elements from the first half of the lanthanide row, such as samarium and neodymium have positive association energies and do not form complexes with oxygen vacancies, while elements from the second half of the lanthanide row, like holmium and erbium, have negative association energies and trap oxygen vacancies [11]. The location of these vacancies in the CeO₂ structure relative to doped rare earth ions like Er³⁺, Yb³⁺ or Nd³⁺ can be determined using electron paramagnetic resonance spectroscopy (EPR), which is an effective tool for analyzing a comparative low concentration of doped ions ($\leq 1\%$). Indeed, EPR spectra due to cubic centers in the CeO₂ structure indicate the remote location of vacancies, while EPR lines from axial centers point out to the location

[†]This paper is dedicated to Professor Boris Z. Malkin, who made a significant contribution to the field of magnetic radio spectroscopy in Kazan University, on the occasion of his 85th birthday.

of vacancies in the close environment of a paramagnetic center. Note that the concentrations of rare earth ions greater than 1% lead to the broadening of the resonance lines due to dipole-dipole interactions between doped ions, and fine details of the EPR spectrum may be lost. Recently we have published the results of EPR studies on CeO₂ NPs doped with a low concentration of Er³⁺ ions ($\leq 0.1\%$), and it has been found that at this concentration, the Er³⁺ ions occupy mainly cubic sites [16,17]. Here we present the results for a higher concentration of Er³⁺ ions, to study the effect of annealing conditions on the local structure of the rare earth ions in CeO₂ : 1% Er³⁺ nanoparticles.

2. Experimental techniques

The phase composition of the powders was studied by X-ray diffraction method (XRD) using Bruker D8 Advance X-ray diffractometer (Cu K α radiation $\lambda = 0.154$ nm).

The EPR measurements were conducted using a continuous wave spectrometer operating at ~ 9.4 GHz (X-band, Bruker ESP-300). The modulation frequency was 100 kHz and the modulation amplitude was 1 G, the power level varied within of 2.5 – 25 mW. Low temperatures were obtained using a commercial liquid-helium flow cryostat system (Oxford Instruments).

Magnetization measurements were carried out at room temperatures using the Quantum Design Physical Property Measurement System (PPMS-9, USA) with the vibrating sample option of the magnetometer. The sensitivity of device was better than 10^{-6} emu at a data rate of 1 Hz.

Optical spectra were studied using Horiba Fluorolog QM spectrofluorimeter and StellarNet CCD spectrometer.

3. Samples preparation and their characterization

Nanoparticles of CeO₂ were prepared using the coprecipitation method from aqueous solution of cerium (III) nitrate hexahydrate (Ce(NO₃)₃*6H₂O), the erbium (III) nitrate pentahydrate (Er(NO₃)₃*5H₂O) powders and hexamethylenetetramine (CH₂)₆N₄, (HMTA) [18–20]. The erbium (III) nitrate pentahydrate had purity 99.9% and was taken in the amount to obtain 1 mol.% of Er³⁺ ions in CeO₂ nanoparticles. Aqueous solutions of Ce(NO₃)₃*6H₂O (purity 99.9%)+Er(NO₃)₃*5H₂O and HMTA (purity 99.99%) were filtered and then mixed and kept at room temperature for 15 hours. Then, the solution was heated up to 60°C and kept at this temperature for an hour during which the mixture was stirred on a magnetic stirrer. The acidity of the solution was kept at pH = 6 throughout the process. After the heating, the solution was cooled down during 24 hours.

The precipitated oxides were collected by centrifugation of the mixture at a rate of 9000 rpm for 10 min. Then the solution was drained, and the particles remaining at the bottom were broken up using an ultrasonic bath for half an hour. The washing process was repeated 5 times. The resulting nano powder was dried at 50°C for 24 hours, it was notated as the initial powder and was used to prepare 3 different samples. The sample #1 was obtained by annealing the initial powder under air at 600°C for 4 hours in the muffle furnace, the sample #2 was obtained by annealing the powder in argon atmosphere at 600°C for 2 hours, and the sample #3 was obtained by annealing the powder in the vacuum (at $\sim 10^{-4}$ mbar) at 1000°C for 2 hours.

Notations of the prepared samples are given in the Table 1. XRD spectra of the CeO₂ : 1% Er³⁺ NPs samples are shown in Figure 1. Analysis of the obtained spectra shows the crystalline structure of CeO₂, with no other phases detected. Simulations and calculations of the XRD peaks were carried out using the Vesta software [21].

Table 1. Notations and annealing conditions of studied samples

Sample notation	Composition	Annealing temperature, atmosphere and duration
#1	CeO ₂ : 1% Er ³⁺	600°C, air, 4 hours
#2		600°C, argon, 2 hours
#3		1000°C, vacuum, 2 hours

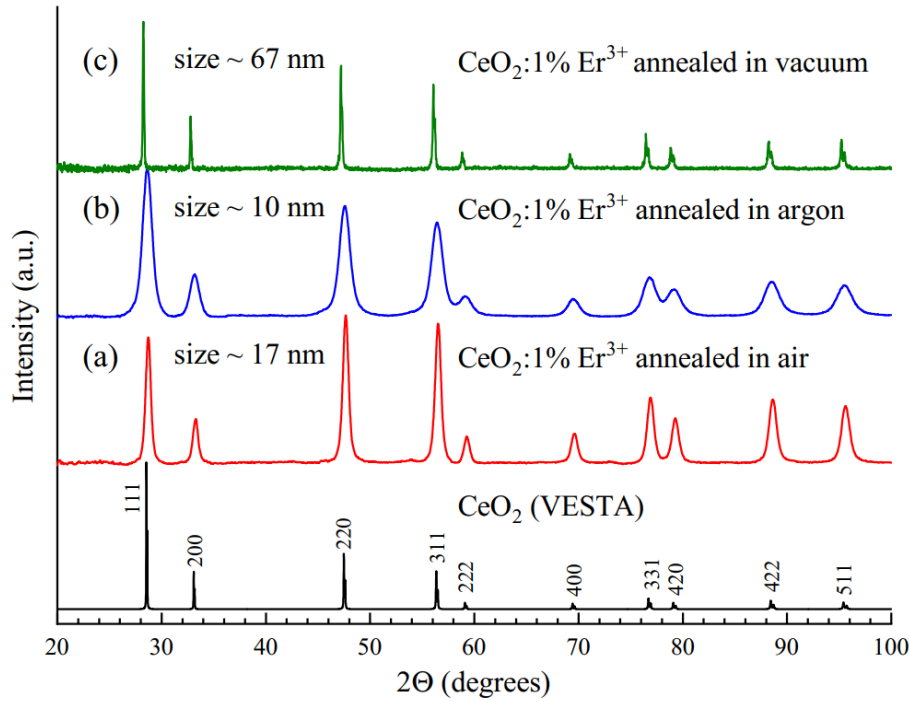


Figure 1. XRD spectra of studied samples. a) sample #1, b) sample #2, c) sample #3.

The size of the NPs was estimated from the XRD lines using the Scherrer equation [22]

$$D = \frac{K\lambda}{\beta_D \cos \theta} \quad (1)$$

where D represents the coherent scattering domains (CSD) size, K is the particle shape-factor (0.9), λ is the X-ray wavelength of Cu K α radiation (0.154 nm), β_D is the full width at half maximum (FWHM) of the XRD (111) diffraction peak in radians, and θ is the Bragg diffraction angle in degree. The estimated average nanoparticle size for samples annealed in air is ~ 17 nm, those annealed in argon are ~ 10 nm, and those annealed in vacuum are ~ 67 nm.

4. Results and discussion

Luminescence spectra of Er³⁺ doped CeO₂ NPs were previously studied in refs. [16, 17, 23]. As mentioned in ref. [16] the optical properties of these nanoparticles are determined by the optical transitions of the Er³⁺ and Ce³⁺ ions. A corresponding energy level diagram for the Ce³⁺/Er³⁺ system is presented in Figure 2a.

The Ce³⁺ ion has a 4f ground state configuration and a low excited 5d state. Ce³⁺ ions placed in a crystal field have allowed 4f \rightarrow 5d electric dipole transitions and can be observed in the wavelength range from 250 to 500 nm, depending on the matrix and the local symmetry of

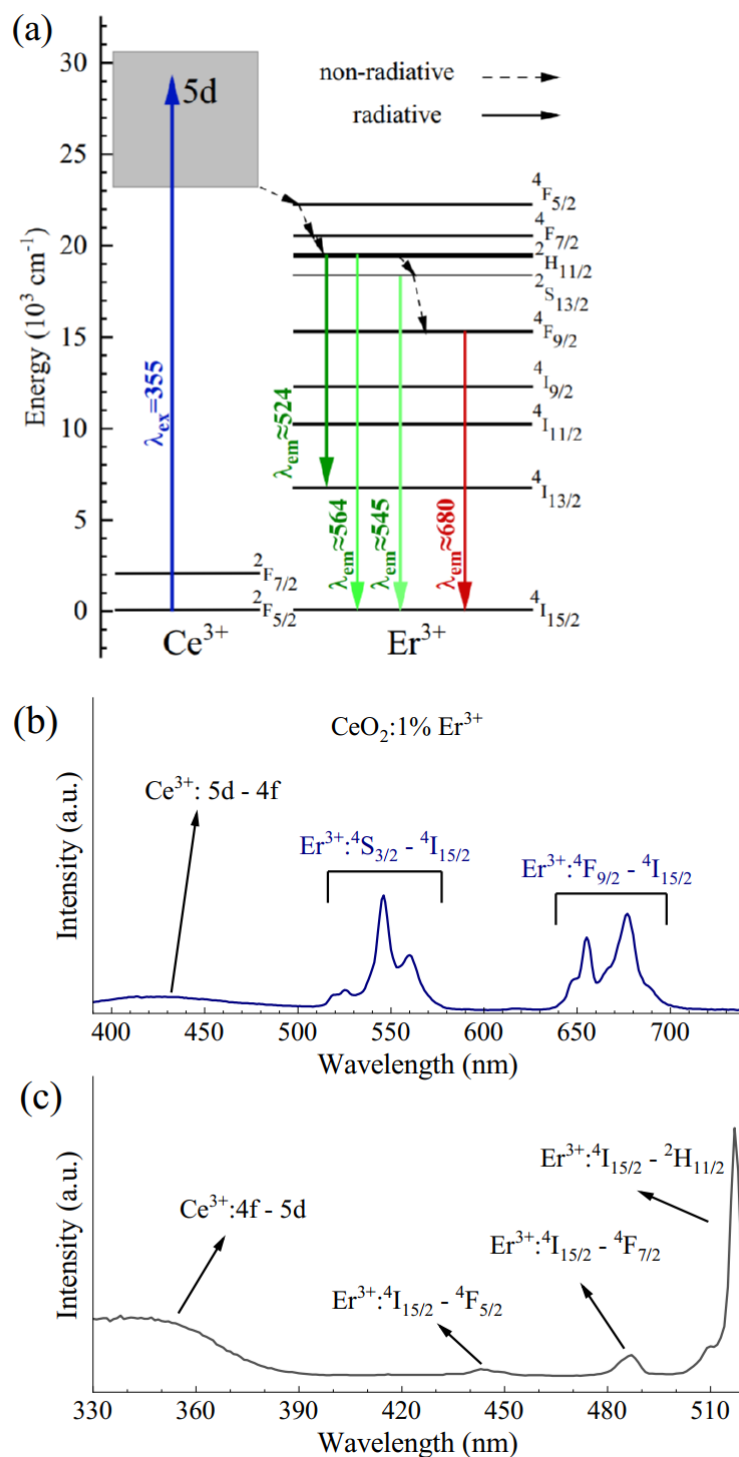


Figure 2. a) The energy level diagram of Ce³⁺/Er³⁺ system with the observed transitions. b) Luminescence spectrum of CeO₂ : 1% Er³⁺, sample #1, excitation at λ_{ex} = 355 nm, room temperature. c) Excitation spectrum for λ_{em} = 545.5 nm (Er³⁺, ⁴S_{3/2} - ⁴I_{15/2} transition) at room temperature.

the impurity ion. The ground 4f state is split by the spin-orbit interaction into two manifolds: the ²F_{5/2} and the ⁵F_{7/2} levels. The excited 5d state of the Ce³⁺ ion has an unshielded electron shell, which is under the influence of a crystal field. Therefore, interconfiguration radiative transitions 5d → 4f of the Ce³⁺ ion, due to their predominantly electric dipole nature, manifest

themselves as intense broad luminescence bands with a short decay time. In contrast, the Er^{3+} ions energy states are belong to 4f-configuration, which is well-shielded from the crystal field by the outer electronic shells, and the 4f-4f electronic transitions are characterized by numerous narrow lines.

Figure 2b shows the luminescence spectrum of sample #1 under the excitation wavelength of 355 nm, which corresponds to the 4f-5d absorption band of the Ce^{3+} ion. Groups of intense lines corresponding to 4f-4f transitions of the Er^{3+} ion are observed in this spectrum. In particular, intense luminescence bands in the wavelength ranges 509 – 534.5 nm, 534.5 – 572.5 nm, and 635 – 702.5 nm are associated with the ${}^2\text{H}_{11/2}-{}^4\text{I}_{15/2}$, ${}^4\text{S}_{3/2}-{}^4\text{I}_{15/2}$, ${}^4\text{F}_{9/2}-{}^4\text{I}_{15/2}$ electronic transitions of the Er^{3+} ion.

The luminescence excitation spectrum of the Er^{3+} ion recorded at a wavelength of 545.5 nm is presented in Figure 2c. This excitation spectrum is characterized by a wide band in the range of approximately 330 – 400 nm, which is associated with the absorption band of the Ce^{3+} 5d state. Additionally, the luminescence of Er^{3+} ions can be excited into the narrow absorption bands of the ${}^4\text{I}_{15/2}-{}^4\text{F}_{5/2}$, ${}^4\text{F}_{7/2}$ or ${}^2\text{H}_{11/2}$ transitions of Er^{3+} ions.

We observed that the luminescence was absent in samples annealed in argon or vacuum. We attribute this to the formation of defects during the annealing process. In contrast, air annealing results in a decrease in the number of these defects. The EPR spectra of the CeO_2

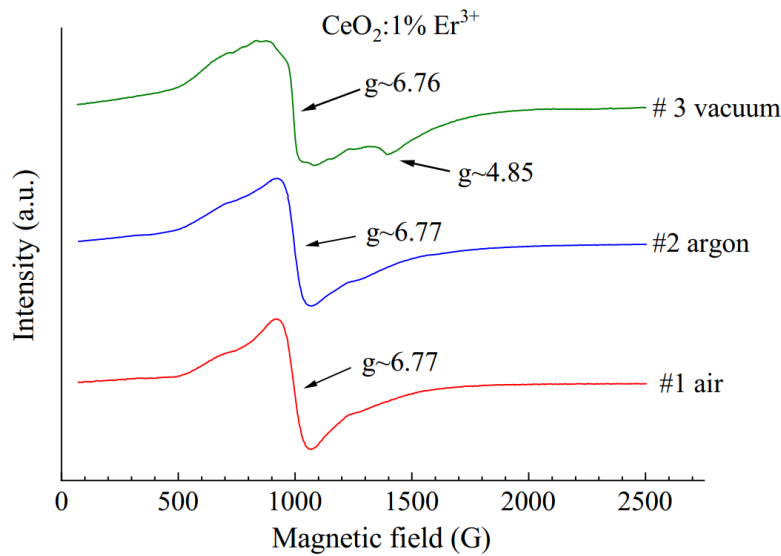


Figure 3. X-band cw EPR spectra of $\text{CeO}_2 : 1\% \text{Er}^{3+}$ NPs at 15 K.

NPs samples are displayed in Figure 3. The absorption line with a g -value of approximately 6.76 – 6.77 is due to cubic centers, which have been previously observed in CeO_2 NPs samples with a lower concentration of Er^{3+} ions [16, 17, 24]. The cubic centers of Er^{3+} ions in the bulk CeO_2 crystal have been studied by other authors [25, 26] who reported the observation of an isotropic line corresponding to even isotopes of erbium with very similar values of g , namely $g = 6.759 \pm 0.005$ [25] and $g = 6.747 \pm 0.006$ [26], respectively. The EPR linewidths of Er^{3+} ions in all samples are quite large due to the broadening caused by dipolar interactions and defects structure in the nanoparticles. This is why no resolved hyperfine structures were observed due to presence of odd isotopes of Er^{3+} ions. The line with $g \sim 4.85$ in the Figure 3 for the sample #3 we assigned to the trigonal center because its g -value is similar to the observed $g \sim 4.84$ for the trigonal center in CeO_2 NPs doped with 0.1% Er^{3+} ions. Previous studies have shown [9]

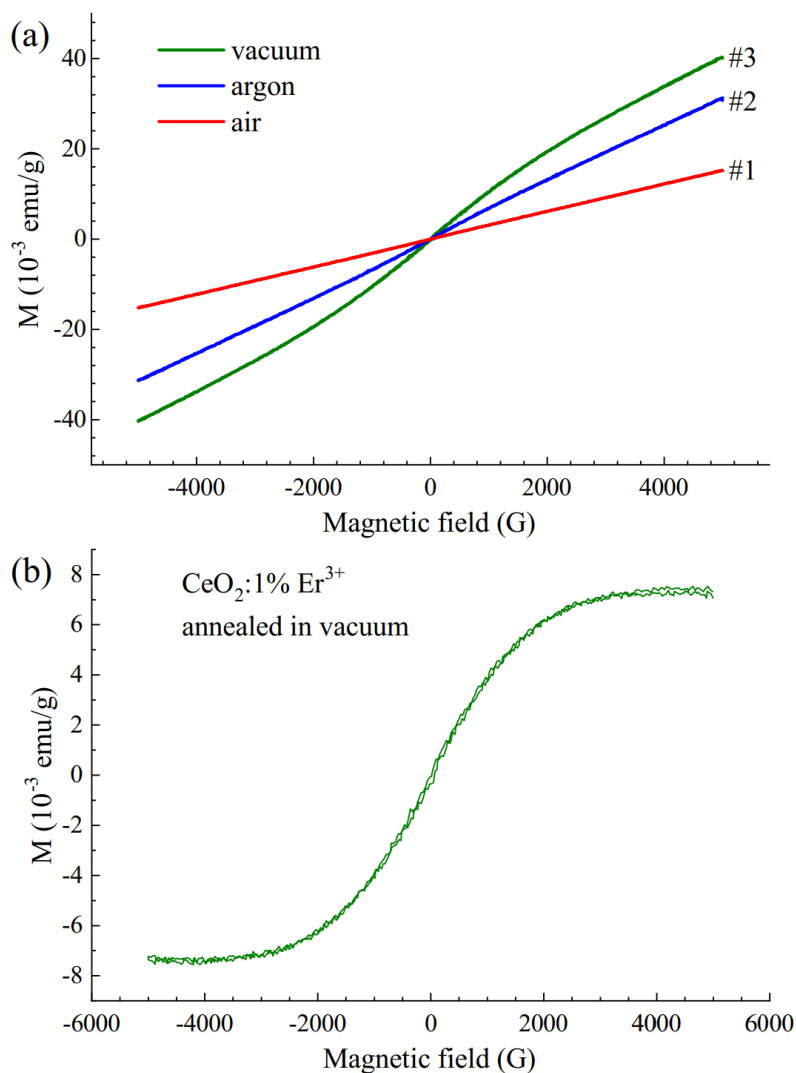


Figure 4. a) M–H dependences of the CeO₂ : 1% Er³⁺ nanopowder samples annealed in air (#1), in argon (#2) and in vacuum (#3) . b) M–H dependence of the sample #3 after subtracting the paramagnetic contribution.

that the annealing CeO₂ in a reduced atmosphere leads to the release of oxygen from the crystal structure, resulting in the formation of oxygen vacancies. The structure of the trigonal centers of Er³⁺ ions in bulk CeO₂ crystal has been discussed in literature [26] but a clear model has not been established. The trigonal symmetry centers are formed due to defects along the $\langle 111 \rangle$ axis of the crystalline structure, which could be oxygen vacancies or hydroxyl groups. It should be noted that the EPR spectra of trigonal centers in the bulk CeO₂ crystal have been reported by M.M. Abraham et al. [26] who give $g_{\parallel} = 10.25 \pm 0.05$, $g_{\perp} = 4.847 \pm 0.005$ and by A.A. Antipin et al. [27] who give $g_{\parallel} = 10.3 \pm 0.05$, $g_{\perp} = 4.84 \pm 0.02$. It should be underlined that for the powder EPR spectra of axial sites with a random orientation of particles the line with g_{\perp} should be much more intensive as compare with g_{\parallel} due to statistical consideration [28,29] and may be the only detectable line in a powder sample. Thus, EPR measurements clearly show the presence of trigonal centers after annealing CeO₂ NPs in a reduced atmosphere that indicates on the oxygen vacancy formation in the nearest environment of Er³⁺ ion.

The oxygen vacancies in undoped and transition metal doped CeO₂ NPs have been associated with room-temperature magnetism (RTM) observed in nonmagnetic oxide NPs [30,31].

The room-temperature magnetism in CeO₂ NPs has been studied and reported in numerous works, and analyzed in the review [31], however the origin of this phenomenon is still not fully understood. The theoretical models proposed to explain the RTM in non-magnetic oxide nanoparticles are either directly related to oxygen vacancies, such as the F-center exchange model [32] or related to charged defects on the nanoparticle surface, including charge transfer ferromagnetism [33] and collective spin response due to giant orbital paramagnetism [34]. However, most publications have shown that oxygen vacancies play a crucial role in RTM.

The dependence of the magnetic moment (M) on the magnetic field for the studied samples is shown in Figure 4a. Samples #1 and #2 exhibit a linear dependence of M on the magnetic field, indicating paramagnetic behavior. The sample #3, on the other hand, shows a dependence typical of ferromagnetic-like behavior in CeO₂ NPs [30,31]. Figure 4b presents the M – H curve for the sample #3 after subtracting the paramagnetic contribution. The saturation magnetization value $M_s \sim 7.4 \cdot 10^{-3}$ emu/g is similar to the values previously observed for the undoped and transition metal doped CeO₂ NPs [35–37].

Thus, EPR and magnetization measurements clearly indicate that the origin of the ferromagnetic-like behavior in CeO₂ NPs is due to vacancies.

5. Conclusions

The CeO₂ nanoparticles doped with 1% Er³⁺ were synthesized using the coprecipitation method from an aqueous solution. In this study, the nanoparticles were analyzed using XRD, as well as optical, EPR, and magnetization techniques. The CeO₂ nanoparticles were subjected to different annealing processes: 4 hours in air at 600°C, 2 hours in argon at 600°C, and 2 hours in vacuum at 1000°C. Luminescence was only observed in the sample annealed in air, while was not present in samples annealed in argon and vacuum. This can be attributed to the defects that formed during the annealing process in the latter two samples. EPR measurements confirmed the presence of trigonal centers after annealing CeO₂ nanoparticles in vacuum indicating the formation of oxygen vacancies in the nearest environment of Er³⁺ ion.

Magnetization measurements displayed a ferromagnetic-like behavior in the CeO₂ : 1% Er³⁺ nanoparticles annealed in vacuum, which correlates with the vacancies formed in this sample. On the other hand, the samples annealed in air and argon exhibited a paramagnetic dependence of magnetic moment on the magnetic field.

Acknowledgments

The work was funded by the grant from the Russian Science Foundation number 22-72-00129 <https://rscf.ru/project/22-72-00129>

The authors gratefully acknowledge the CSF-SAC FRC KSC RAS for providing necessary facilities to carry out optical measurements. The authors are grateful to R.G. Batulin and M.A. Cherosov for the help with magnetization measurements.

References

1. Sun C., Li H., Chen L., *Energy Environ. Sci.* **5**, 8475 (2012).
2. Ahn S.-Y., Jang W.-J., Shim J.-O., Jeon B.-H., Roh H.-S., *Catal. Rev.* , 1 (2023).
3. Walkey C., Das S., Seal S., Erlichman J., Heckman K., Ghibelli L., Traversa E., McGinnis J. F., Self W. T., *Environ. Sci.: Nano* **2**, 33 (2015).

4. Rubio L., Marcos R., Hernández A., *Chem.-Biol. Interact.* **291**, 7 (2018).
5. Thakur N., Manna P., Das J., *J. Nanobiotech.* **17**, 84 (2019).
6. Casals E., Zeng M., Parra-Robert M., Fernández-Varo G., Morales-Ruiz M., Jimenez W., Puentes V., Casals G., *Small* **16**, 1907322 (2020).
7. Kusmirek E., *Catalysts* **10**, 1435 (2020).
8. Gupta K. K., Weng T.-H., Som S., Lu C.-H., *Ceram. Internat.* **49**, 32758 (2023).
9. Trovarelli A., *Catal. Rev.* **38**, 439 (1996).
10. Skorodumova N. V., Simak S. I., Lundqvist B. I., Abrikosov I. A., Johansson B., *Phys. Rev. Lett.* **89**, 166601 (2002).
11. Shehata N., Meehan K., Hudait M., Jain N., *J. Nanopart. Res.* **14**, 1173 (2012).
12. Soni S., Kumar S., Dalela B., Kumar S., Alvi P. A., Dalela S., *J. Alloys and Comp.* **752**, 520 (2018).
13. D'Angelo A. M., Liu A. C. Y., Chaffee A. L., *J. Phys. Chem. C* **120**, 14382 (2016).
14. Guo M., Lu J., Wu Y., Wang Y., Luo M., *Langmuir* **27**, 3872 (2011).
15. Schmitt R., Nenning A., Kraynis O., Korobko R., Frenkel A. I., Lubomirsky I., Haile S. M., Rupp J. L. M., *Chem. Soc. Rev.* **49**, 554 (2020).
16. Pudovkin M. S., Morozov O. A., Korableva S. L., Rakhmatullin R. M., Semashko V. V., Ginkel A. K., Rodionov A. A., Kiiamov A. G., *Ceram. Internat.* **50**, 9263 (2024).
17. Rakhmatullin R. M., Kurkin I. N., Pavlov V. V., Semashko V. V., *Phys. Status Solid. (b)* **251**, 1545 (2014).
18. Chen P.-L., Chen I.-W., *J. Amer. Ceram. Soc.* **76**, 1577 (1993).
19. Zhang F., Jin Q., Chan S.-W., *J. Appl. Phys.* **95**, 4319 (2004).
20. Polezhaeva O. S., Yaroshinskaya N. V., Ivanov V. K., *Inorg. Mater.* **44**, 51 (2008).
21. Momma K., Izumi F., *J. Appl. Crystall.* **44**, 1272 (2011).
22. Holzwarth U., Gibson N., *Nature Nanotech.* **6**, 534 (2011).
23. Yang Y., Cong Y., Dong D. P., Xiao Y., Shang J. Y., Tong Y., Zhang H. M., He M., Zhang J. H., *J. Lumin.* **213**, 427 (2019).
24. Rakhmatullin R. M., Aminov L. K., Kurkin I. N., Poepl A., *Appl. Magn. Res.* **46**, 741 (2015).
25. Komet Y., Low W., Linares R., *Phys. Lett.* **19**, 473 (1965).
26. Abraham M. M., Weeks R. A., Clark G. W., Finch C. B., *Phys. Rev.* **148**, 350 (1966).
27. Antipin A. A., Zonn Z. N., Ioffe V. A., Katyshev A. N., Shekun L. Y., *Sov. Phys. Solid State* **9**, 521 (1967).

28. Abragam A., Bleaney B., *Electron Paramagnetic Resonance of Transition Ions* (Clarendon Press, Oxford, 1970) 911 p.
29. Weil J. A., Bolton J. R., *Electron paramagnetic resonance: elementary theory and practical applications*, 2nd ed. (John Wiley & Sons, Hoboken, New Jersey, 2007) 688 p.
30. Sundaresan A., Bhargavi R., Rangarajan N., Siddesh U., Rao C. N. R., *Phys. Rev. B* **74**, 161306 (2006).
31. Ackland K., Coe J. M. D., *Phys. Rep.* **746**, 1 (2018).
32. Coey J. M. D., Venkatesan M., Fitzgerald C. B., *Nature Mater.* **4**, 173 (2005).
33. Coey J. M. D., Wongsaprom K., Alaria J., Venkatesan M., *J. Phys. D* **41**, 134012 (2008).
34. Coey M., Ackland K., Venkatesan M., Sen S., *Nature Phys.* **12**, 694 (2016).
35. Rakhmatullin R. M., Pavlov V. V., Semashko V. V., *Phys. Status Solid. (b)* **253**, 499 (2018).
36. Morozov O. A., Pavlov V. V., Rakhmatullin R. M., Semashko V. V., Korableva S. L., *Phys. Status Solid. (RRL)* **12**, 1800318 (2018).
37. Rakhmatullin R. M., Semashko V. V., Korableva S. L., Kiiamov A. G., Rodionov A. A., Tschaggelar R., van Bokhoven J. A., Paun C., *Material. Chem. Phys.* **219**, 251 (2018).